LA-UR- 08-7925

Approved for public release;
distribution is unlimited.

Title:	Electrokinetic transport in microchannels with random roughness
Author(s):	Moran Wang Qinjun Kang
Intended for:	Publication in Analytical Chemistry

Los Alamos
NATIONAL LABORATORY
EST.1943

Form 836 (7/06)

Electrokinetic transport in microchannels with random roughness

Moran Wang[1] *and Qinjun Kang*[1]

Computational Earth Science Group (EES-16)

Los Alamos National Laboratory, Los Alamos, NM 87545

---

[1] Email address: mwang@lanl.gov (M.W.); qkang@lanl.gov (Q.K)

Abstract: We present a numerical framework to model the electrokinetic transport in microchannels with random roughness. The three-dimensional microstructure of the rough channel is generated by a random generation-growth method with three statistical parameters to control the number density, the total volume fraction and anisotropy characteristics of roughness elements. The governing equations for the electrokinetic transport are solved by a high-efficiency lattice Poisson-Boltzmann method in complex geometries. The effects from the geometric characteristics of roughness on the electrokinetic transport in microchannels are therefore modeled and analyzed. For a given total roughness volume fraction, a higher number density leads to a lower fluctuation due to the random factors. The electroosmotic permeability increases with the roughness number density nearly at a logarithmic law for a given volume fraction of roughness, but decreases with the volume fraction of roughness for a given roughness number density. When both the volume fraction and the number density of roughness are given, the electroosmotic permeability is enhanced by increases of the characteristic length along the external electric field direction or decreases of the length of the direction of across the channel. For a given microstructure of rough microchannel, the electroosmotic permeability decreases with the Debye length. Compared with the corresponding flows in a smooth channel, the rough surface may enhance the electrokinetic transport when the Debye length is smaller than the roughness characteristic height under the assumption of constant zeta potential for all surfaces. The present results may improve the understanding of the electrokinetic transport characteristics in microchannels.

Keywords: electrokinetic transport; rough channel; lattice Boltzmann method; random roughness

I. Introduction

When the length scale is down to micro- and nanometers, the interfacial phenomena become more and more important[1, 2]. The electrokinetic transport, as a classical interfacial phenomenon discovered more than 200 years ago, now plays a fundamental role for a better understanding of liquid flow mechanism through microchannels[3], and hence for optimal design and operation of Microsystems, such as Lab-on-a-chip devices[4, 5] and micro fuel cells[6-8]. At the same time, electrokinetic flow has become one of the most important non-mechanical actuating techniques in microfluidics, used for pumping[9-12], mixing[13-15] and separating[16] etc., due to its excellent scalability, low dispersion and easy of control[4, 10, 13, 17]. Therefore, analysis and modeling of electrokinetic transport in microchannels have recently received a great amount of attention[18-25].

Almost all surfaces have certain degree of roughness either incurred during fabrication process or due to the adsorption/adhesion of other species such as macromolecules. Although it is well known that the electrokinetic flow is sensitive to the surface properties[26], little attention has been paid to the effects of surface roughness on electrokinetic transport due to its complexity, especially for random roughness in microchannels[27].

Dukhin and Derjaguin [28] may be the first ones who performed systematic theoretical studies on roughness effects on electrokinetic flows. They introduced two critical length scales to characterize the problem: the Debye length which is defined as the thickness of the electrical double layer, and the charactertistic length of surface roughness. For thin double layer cases where the Debye length is much smaller than the surface roughness height, the electroosmotic flow near the concave-convex portion of the rough surface is essentially the same as that near a smooth surface, and the Smoluchowski equation is therefore valid. The electroosmotic flow in a rough channel can thus be predicted by the standard linear models. When the Debye length is

comparable to the roughness height, the linearized models fail to describe the electrokinetic transport any more. Especially when the Debye length is much larger than the roughness size, the effective charge density on the rough surfaces is higher than the corresponding smooth surfaces due to the increased area by the roughness[26].

Thanks to the rapid development of computer and computational techniques, a few numerical approaches have been applied to model and predict the electrokinetic transport in rough microchannels. Hu et al. [29-31] studied the electroosmotic flow in microchannels with three-dimensional rectangular roughness elements using a finite-volume-based numerical model within a thin Debye length limit. Finite element method and analysis have been employed as well to investigate the electroosmotic flow in microchannels with two-dimensional sinusoidal roughness [32, 33]. Recently, a lattice Poisson-Boltzmann method (LPBM) has been proposed to use as an efficient solver for the strongly nonlinear governing equations for electrokinetic flows in microchannels [24] and the two-dimensional rectangular roughness and cavitation effects have been investigated [34]. Up to now the electrokinetic flows in microchannels with random roughness have never been studied to the best knowledge of the authors.

There are two challenges to model the electrokinetic flows in microchannels with random roughness. The first one is how to describe the complex geometries of random roughness in microchannels. In most cases the roughness in a real microchannel caused by manufacture or macromolecules adsorption is out of control, which means that the roughness geometry features, such as position, shape and size, are irregular and random. Since the electrokinetic flows are sensitive to surface characteristics, any imitation with regular geometry for roughness may lead to inaccurate predictions and analysis to a real system. However there is no effective way in the existing literature for digitalizing the complex geometries of random roughness in microchannels

yet. Secondly, solving the governing equations efficiently for electrokinetic flow in complex geometries is still very challenging. The coupled electrostatic, hydrodynamic and mass transport problem subject to complex geometrical boundary conditions represented by the solid-liquid interface in randomly rough channels requires huge or even unacceptable computational resources for the traditional partial differential equation (PDE) solvers, such as the finite difference method (FDM) and the finite element method (FEM). The difficulty mainly comes from two aspects: the strong nonlinearity of governing equations and the irregularity of random structures. The former may cause the classical PDE solvers unstable or even disconvergent, while the latter will lead to a requirement for extreme grid refinements in the computational domain especially near the roughness. This computational difficulty in traditional PDE solvers thus limited modeling and analysis of electrokinetic flow to very simple geometries.

Facing these challenges, we are aiming to (1) build up a numerical framework for modeling electrokinetic transport in microchannels with random roughness; (2) analyze the effects of roughness geometry on the electrodynamic and hydrodynamic transport in microchannels. The results will be compared with the existing theoretical analysis and numerical data.

II. Mathematical models

Consider an N -component Newtonian electrolyte flowing with a velocity $\mathbf{u}(\mathbf{r},t)$ in microchannels with no polarization or chemical reactions. Let $\psi(\mathbf{r},t)$ be the electric potential prevailing within the solution where $\mathbf{r}$ is the position vector; the flux $\mathbf{J}_i$ of each ith ion species, composing the solute, is given by the following constitutive equation [26, 35]:

$$\mathbf{J}_i = -D_i \nabla n_i - \frac{ez_i D_i n_i}{kT} \nabla \psi + n_i \mathbf{u}, \tag{1}$$

where n_i is the number density of the ith ion species, z_i the ith ion algebraic valence, and e the absolute charge of electron, D_i the ion's diffusivity, k the Boltzmann constant and T the absolute temperature. The ionic flux $\mathbf{J}_i$ and the concentration n_i obey the equation

$$\frac{\partial n_i}{\partial t} + \nabla \cdot \mathbf{J}_i = 0. \tag{2}$$

For an incompressible laminar electroosmotic flow, the movement of fluid is governed by the continuity and momentum equations:

$$\nabla \cdot \mathbf{u} = 0, \tag{3}$$

$$\rho \frac{\partial \mathbf{u}}{\partial t} + \rho \mathbf{u} \cdot \nabla \mathbf{u} = \mu \nabla^2 \mathbf{u} + \mathbf{F}, \tag{4}$$

where ρ is the fluid density, and μ the dynamic fluid viscosity. $\mathbf{F}$ can be any kind of body force but here we only consider the driving force from the electric field. In general, the electric force in electrokinetic fluids may include the Lorentz force associated with external applied electric field, the force caused by the electromagnetic susceptibility, and the intermolecular electric attraction [24]. In the present contribution, we are considering vey slow quasi-steady-state-electrokinetic flow in microchannels so that the other forces except the static electric force are negligible. Therefore the driving force is simplified as:

$$\mathbf{F} = \rho_e \mathbf{E}, \tag{5}$$

where ρ_e is the net charge density and $\mathbf{E}$ is the electric field strength. The net charge density ρ_e can be expressed as

$$\rho_e = \sum_i e z_i n_i. \tag{6}$$

The electric potential distribution is governed by the Poisson equation

$$\nabla^2\psi = -\frac{\rho_e}{\varepsilon_r\varepsilon_0} = -\frac{1}{\varepsilon_r\varepsilon_0}\sum_{i=1}^{N} en_i z_i , \tag{7}$$

where ε_r is the dimensionless fluid dielectric constant and ε_0 the permittivity of a vacuum.

Equations (2)-(7) are the governing equations for electroosmosis in microchannels and can be solved subject to the following boundary conditions on the liquid-solid interface Ω

$$(\mathbf{v}\cdot\mathbf{J}_i)_\Omega = 0, \tag{8}$$

$$\mathbf{u}_\Omega = 0, \tag{9}$$

$$\psi_\Omega = \zeta , \tag{10}$$

where $\mathbf{v}$ is the outer normal to Ω, and ζ the zeta potential.

When the ionic convection is negligible and the electric potential field is continuously derivable, Eq.(2) has a simple steady solution for dilute electrolyte solutions that the ionic concentration n_i falls into the Boltzmann distribution:

$$n_i = n_{i,\infty}\exp\left(-\frac{ez_i}{kT}\psi\right), \tag{11}$$

where $n_{i,\infty}$ is the bulk ionic number density. Substituting Eq.(11) into Eq.(7) yields the famous nonlinear Poisson-Boltzmann equation for electrokinetic flows [36]:

$$\nabla^2\psi = -\frac{1}{\varepsilon_r\varepsilon_0}\sum_i ez_i n_{i,\infty}\exp\left(-\frac{ez_i}{kT}\psi\right). \tag{12}$$

The present contribution solves the governing equations (3-6,11,12) subject to the boundary conditions Eqs. (8-10) by the numerical methods as described in the next section.

III. Numerical methods

This section describes the numerical methods used to simulate electrokinetic flows in microchannels with random roughness, including a reproduction algorithm for three-dimensional

random roughness microstructures and a mesoscopic PDE solver for the multi-physical transport equations, the lattice Poisson-Boltzmann method.

3.1 Generation of Random Roughness

Although the microstructure details of each roughness element, such as shape, size and connections, are quite random in a real microchannel, people can still measure and summarize essential statistical information of morphology and then generate an equivalent structure in computer. The macroscopic statistical information of random roughness may include: roughness position distribution, roughness element shape and average size, volume fraction of roughness, anisotropy degree of roughness element, and so on. The reproduced roughness microstructure may not have to be exactly the same as the real one in every detail, but may involve most of the same macroscopic structure characteristics in statistics.

A. Description of algorithm

No references have been found to reproduce the random roughness in microchannels yet. Herein inspired by a random generation-growth method for constructing of random microstructures of porous media [37, 38], we adapt it to reproduce microstructures of random roughness on upper and lower smooth walls in a three-dimensional microchannel. The process of the generation-growth model for random roughness microstructures is described as below:

i) Randomly locate seeds of roughness elements on the upper and lower wall surfaces based on a roughness distribution probability, s_d, whose value is no greater than the volume fraction of roughness. Each cell of both walls is assigned a random number by a uniform distribution function within (0, 1). The cell whose random number is no greater than s_d will be chosen as a roughness element seed;

ii) Grow every cell of the existing roughness elements to its neighboring cells to its six directions based on the given directional growth probability, D_j, where j represents the direction. Again for each neighboring cell, new random numbers will be assigned and those cells whose random number is no greater than D_j, will become part of roughness;

iii) Repeat the growing process of (ii) until the volume fraction of the total roughness elements reaches the given value V_R.

Thus the generated microstructure is controlled by the three statistical parameters, s_d, D_j and V_R.

B. Discussion on parameters

The roughness distribution probability, s_d, which is defined as the probability of a cell/grid on the walls to become a seed of roughness, is strongly related to the number density of roughness elements. For a given roughness volume fraction, the number density of roughness elements n_R and the average volume of each roughness element V_{r_e} are related to s_d as:

$$n_R = N_{wall} \cdot s_d / A_{wall} , \tag{13a}$$

$$\overline{V_{r\_e}} = V_R / (2N_{wall} \cdot s_d) , \tag{13b}$$

where N_{wall} and A_{wall} denote the total cell number and area of each wall, respectively.

The value of s_d also controls the degree of structure details for a given volume fraction of roughness and grid systems. A smaller s_d leads to a finer description of the microstructures, including shape and connections of the roughness elements.

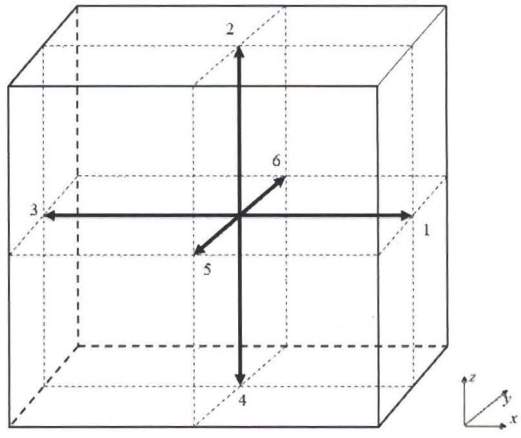

Fig. 1 Six growth directions of each cell in three-dimensional cubic grid systems

The directional growth probability D_j, which is defined as the probability of a cell neighboring in the *j -th* direction to become a part of roughness elements, controls the degree of anisotropy. Different from those for porous media, there are only six growth directions for roughness elements, as shown in Fig. 1, because the roughness can not own independent cells. We can obtain an "isotropic" structure of roughness elements by assign each directional growth probability to the same value. The so-called isotropic structure for a single roughness is a half-spherical structure in statistics. We can vary the anisotropy of roughness structures by changing the relative value, or the ratio in other words, but not the absolute value of the directional growth probabilities. Half-elliptical structures will be generated if the ratio $D_x : D_y : D_z$ does not equal to unit, and the averaged radius ratio is proportional to the square root of the growth probability ratio: $\overline{R_i} \propto \sqrt{D_i}$.

C. Examples

To indicate the roughness shape changing with the directional growth probability, we first generate one single roughness element in the channel by putting only one seed on the middle of the lower wall. Fig. 2 shows three cross section profiles of 3D roughness geometry at the y-

directional middle section (y=30) on a 3D grid system of 60×60×60. The stochastic characteristics of structures are depicted quite realistically in the figures. The blue parts represent the solid roughness and the red the channel. Fig. 2(a) shows a half-sphere-like structure since the growth probabilities in all directions are equal. The structure is therefore isotropic in statistics when standing on its seed position, which means the averaged radius length for each direction is the same. Anisotropic structures are demonstrated in Fig. 2(b) and (c) by change the growth probability ratios. Half-ellipse-like structures are generated. When the z-directional growth probability is four times of the other two ones, the z-directional radius is approximately two times of those in the other directions, as shown in Fig. 2(b). The z-directional radius is statistically half of those in x- and y-directions if its growth probability is a quarter of the other ones (see Fig. 2(c)). These results validate that the characteristic length in each direction is proportional to the square root of its growth probability.

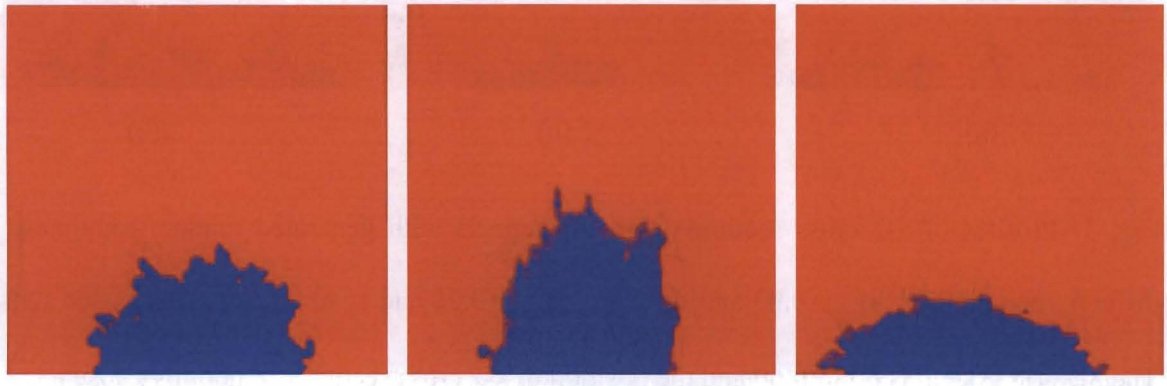

(a) (b) (c)

Fig. 2 Cross section profiles for isotropic or anisotropic structure of single-roughness element. (a) $D_x : D_y : D_z$=1:1:1; (b) $D_x : D_y : D_z$=1:1:4; (c) $D_x : D_y : D_z$=4:4:1. The 3D grid system is 60×60×60 and the cross section position is at the middle of y axis. The volume fraction of roughness V_R=0.05.

Fig. 3 shows effects from the roughness distribution probability and the roughness volume fraction on the geometries and connections in the rough microchannels. The roughness elements are supposed to be isotropic in statistics. The 60×60×60 grid is used and the locations of the x-z cross section profiles are randomly chosen. Comparisons between Fig. 3(a) and (b) indicate that a larger roughness distribution probability leads to more roughness elements with a smaller averaged roughness element size for the same roughness volume fraction. A larger total roughness volume fraction results in larger roughness size and greater roughness connections by comparing Fig. 3(a) with (c).

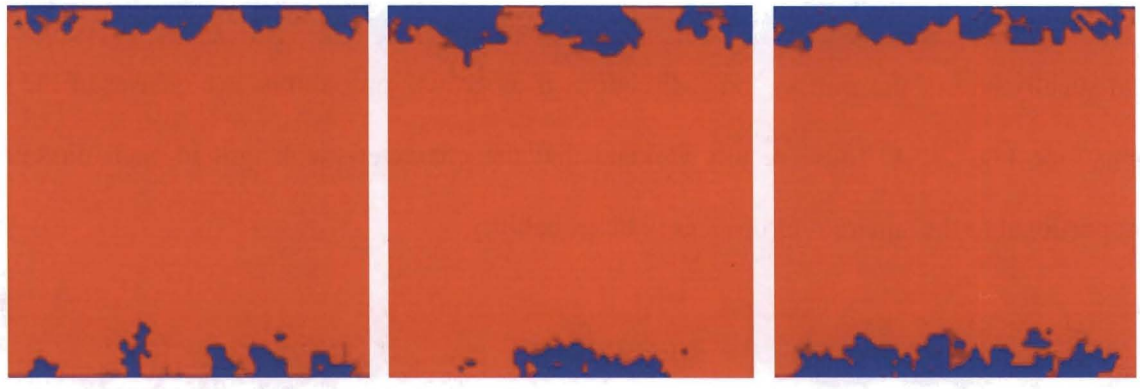

(a) (b) (c)

Fig. 3 Profiles of x-z cross sections in microchannels with generated random roughness for different parameters: (a) s_d=0.03 and V_R=0.06; (b) s_d=0.01 and V_R=0.06; (c) s_d=0.03 and V_R=0.1. The 3D grid system is 60×60×60 and the position of x-z cross section is randomly chosen.

3.2 Lattice Poisson-Boltzmann Method

After the rough channel is generated, the set of coupled hydrodynamic and electrodynamic governing equations for the electrokinetic flows subject to the appropriate boundary conditions will be solved by the LPBM which combines an electric potential evolution on discrete lattices to solve the nonlinear Poisson equation (lattice Poisson method) with a density evolution method

on a same set of discrete lattices to solve the Boltzmann-BGK equation (lattice Boltzmann method) [24]. The equations are only solved in liquid phase and the solid phase is silent and charged homogeneously on the surfaces.

A. Evolution equations

Unlike conventional computational methods based on macroscopic continuum equations, the lattice Boltzmann method employs the mesoscopic Boltzmann equation to determine macroscopic transport dynamics, and solves the governing equations by tracking distribution functions of particle packets on lattices[39]. For laminar flows driven by an external force, the Boltzmann-BGK equation with an external force term, F, is

$$\frac{Df}{Dt} \equiv \partial_t f + (\xi \cdot \nabla) f = -\frac{f - f^{eq}}{\tau_v} + F, \tag{14}$$

where $f \equiv f(x,\xi,t)$ is the single particle distribution function in the phase space (x,ξ), ξ the microscopic velocity, τ_v the relaxation time, f^{eq} the Maxwell-Boltzmann equilibrium distribution and F the external force term

$$F = \frac{3\mathbf{G} \cdot (\xi - \mathbf{u})}{c^2} f^{eq}, \tag{15}$$

where $\mathbf{G}$ is the external force per unit mass [40] and c the lattice speed for mass transfer defined as δ_x/δ_t with δ_x representing the lattice constant (grid size) and δ_t the time step.

Thus the discrete density evolution equation is

$$f_\alpha(\mathbf{r} + \mathbf{e}_\alpha \delta_t, t + \delta_t) - f_\alpha(\mathbf{r},t) = -\frac{1}{\tau_v}\left[f_\alpha(\mathbf{r},t) - f_\alpha^{eq}(\mathbf{r},t)\right] + \delta_t F_\alpha, \tag{16}$$

where $\mathbf{e}_\alpha$ denote the discrete velocities, τ_v the dimensionless relaxation time, and f_α^{eq} the density equilibrium distribution. For a three-dimensional fifteen-speed (D3Q15) system shown in Fig. 4,

$$\mathbf{e}_\alpha = \begin{cases} (0,0,0) & \alpha = 0 \\ (\pm 1,0,0)c,(0,\pm 1,0)c,(0,0,\pm 1)c & \alpha = 1\ to\ 6 \\ (\pm 1,\pm 1,\pm 1)c & \alpha = 7\ to\ 14 \end{cases}, \tag{17}$$

the dimensionless relaxation time which is a function of the fluid viscosity,

$$\tau_\nu = \frac{3\nu}{\delta_x c} + 0.5, \tag{18}$$

with ν representing the kinetic viscosity, and

$$f_\alpha^{eq} = \omega_\alpha \rho \left[1 + 3\frac{\mathbf{e}_\alpha \cdot \mathbf{u}}{c^2} + 9\frac{(\mathbf{e}_\alpha \cdot \mathbf{u})^2}{2c^4} - \frac{3\mathbf{u}^2}{2c^2} \right], \tag{19}$$

with

$$\omega_\alpha = \begin{cases} 2/9 & \alpha = 0 \\ 1/9 & \alpha = 1\ to\ 6 \\ 1/72 & \alpha = 7\ to\ 14 \end{cases}. \tag{20}$$

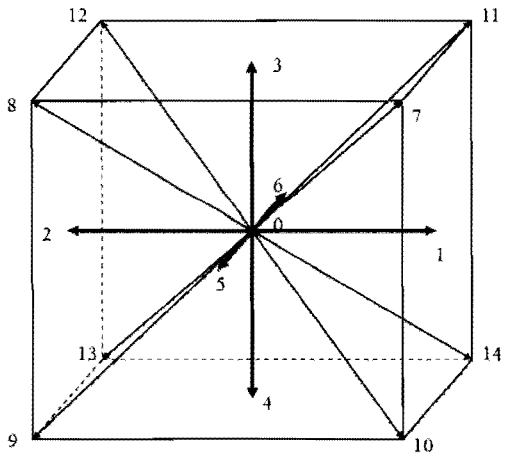

Fig. 4 The lattice direction system (α) for D3Q15 model

The external force in the discrete evolution equation is

$$F_\alpha = \frac{3\rho_e \mathbf{E} \cdot (\mathbf{e}_\alpha - \mathbf{u})}{\rho c^2} f_\alpha^{eq}. \tag{22}$$

The macroscopic density and velocity can be calculated using

$$\rho = \sum_{\alpha} f_{\alpha}, \tag{23}$$

$$\rho \mathbf{u} = \sum_{\alpha} \mathbf{e}_{\alpha} f_{\alpha}. \tag{24}$$

To solve the Poisson equation with strong nonlinearity, Eq. (12), we employ here another evolution method on the same grid system, the lattice Poisson method (LPM) [24, 41], by tracking the electric potential distribution transporting on the discrete lattices. First we extend Eq. (12) into a time-dependent form

$$\frac{\partial \psi}{\partial t} = \nabla^2 \psi + g_{rhs}(\mathbf{r}, \psi, t), \tag{25}$$

with $g_{rhs} = \frac{1}{\varepsilon \varepsilon_0} \sum_i z_i e n_{i,\infty} \exp\left(-\frac{z_i e}{k_b T} \psi \right)$ representing the *opposite* of the right hand side (RHS) of the original Eq. (12), and then we adopt the following discrete evolution equation for the electric potential distribution [24, 41]

$$g_{\alpha}(\mathbf{r} + \Delta \mathbf{r}, t + \delta_{t,g}) - g_{\alpha}(\mathbf{r}, t) = -\frac{1}{\tau_g}\left[g_{\alpha}(\mathbf{r}, t) - g_{\alpha}^{eq}(\mathbf{r}, t) \right] + (1 - \frac{0.5}{\tau_g}) \delta_{t,g} \omega_{\alpha} g_{rhs}, \tag{26}$$

where the equilibrium distribution of the electric potential evolution variable g is

$$g_{\alpha}^{eq} = \begin{cases} 0 & \alpha = 0 \\ \psi / 9 & \alpha = 1 \, to \, 6 \\ \psi / 24 & \alpha = 7 \, to \, 14 \end{cases}. \tag{27}$$

The time step for the electric potential evolution is

$$\delta_{t,g} = \frac{\delta_x}{c_g}, \tag{28}$$

where c_g is the lattice speed for the electric potential propagation [41]. The dimensionless relaxation time is

$$\tau_g = \frac{9}{5\delta_x c_g} + 0.5 . \tag{29}$$

It has been proved that c_g can be any positive number only ensuring the value of τ_g within 0.5 and 2 [41, 42]. After evolving on the discrete lattices, the macroscopic electric potential can be calculated using

$$\psi = \sum_{\alpha} (g_\alpha + 0.5\delta_{t,g} g_{rhs} \omega_\alpha) . \tag{30}$$

Such an evolution equation for electric potential distribution is valid for both steady flows and unsteady flows at very low velocities because the electromagnetic susceptibility effect is ignored in the present form. Although the lattice evolution method for nonlinear Poisson equation is not as efficient as the multi-grid solutions for simple geometries due to its long wavelength limit, it is more suitable for parallel computing and for geometrical complexity [43, 44].

B. Boundary condition treatments

The boundary condition implements are critical to the accuracy of the numerical simulations. The hydrodynamic boundary conditions for the lattice Boltzmann method have been studied extensively[45-48]. The conventional bounce-back rule is the most commonly used method to treat the velocity boundary condition at the solid-fluid interface due to its easy implement, where momentum from an incoming fluid particle is bounced back in the opposite direction as it hits the wall[39]. However the conventional bounce-back rule has two main disadvantages. First, it requires the dimensionless relaxation time strictly within the range of (0.5, 2), otherwise the prediction will deviate from the correct result [45]. Second, the non-slip boundary implemented by the conventional bounce-back rule is not located on the boundary nodes exactly, which will lead to inconsistencies when coupling with other PDE solvers on a same grid set [48]. To overcome the inconsistencies between the LBM and other PDE solvers on a same grid set, one can replace the

bounce-back rule with another "non-slip" boundary treatment proposed by Inamuro et al. [46], with the cost of loss of easy implement for complicated geometries. An alternative solution is to modify the boundary condition treatments of the PDE solver for the electric potential distribution to be consistent with the LBM bounded by the bounce-back rule.

In this contribution, the bounce-back rule for nonequilibrium distribution proposed by Zou and He[47] is introduced and extended to both hydrodynamic and electrodynamic boundary implements to deal with the complex geometries of random roughness.

At the boundary the following hydrodynamic condition holds:

$$f_{\alpha}^{neq} = f_{\beta}^{neq}, \tag{31}$$

where the subscripts α and β represent the opposite directions.

Analogously, the non-equilibrium "bounce-back" rule for the electric potential distribution at the wall surfaces is suggested as:

$$g_{\alpha}^{neq} = -g_{\beta}^{neq}. \tag{32}$$

These boundary treatments are easy to implement for complicated geometries and have approximately second-order accuracy [47, 48].

IV. Results and discussion

Fig. 5 shows a schematic illustration of three dimensional electrokinetic flows in charged rough microchannel. The roughness is randomly distributed on upper and lower walls, which is generated by the algorithm described in section 3.1. The cubic domain is periodic in both x and y directions. The solid surfaces are homogeneously charged with a zeta potential, ζ, and the electrolyte solution is driven flowing through the channel by an external electric field, $\mathbf{E}$.

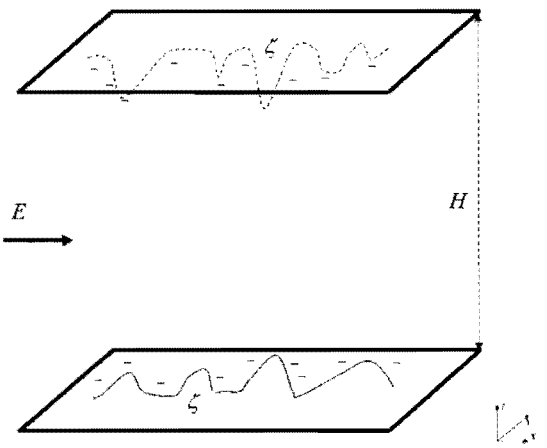

Fig. 5 Schematic of electrokinetic flows in rough microchannel

In the present simulations, the channel width H, which is defined as the distance between the two smooth base walls, is fixed at one micron. A 60×60×60 uniform grid is used. We change the values of generation parameters (s_d, D_i and V_R) to vary the geometries of roughness. The bulk ionic concentration n_∞ is 0.3×10^{-5} M for most cases and may vary from 0.3 to 3.3×10^{-5} M when we need to change the Debye length. The other properties and parameters used in this work are: the fluid density ρ=999.9 kg/m^3, the dielectric constant $\varepsilon_r\varepsilon_0$=$6.95\times10^{-10}$ C^2/J m, the dynamic viscosity μ=0.889 mPa s, the temperature T=273 K, the surface zeta potential -50 mV and the external electric field strength E=1×10^6 V/m.

A. Roughness number density effect

First we consider the effects from the roughness number density n_R for a given total roughness volume fraction at V_R=0.05. Supposing the roughness elements are isotropic, we vary the roughness number density by changing the value of the roughness distribution probability s_d, and n_R is then calculated through Eq.(13a).

Fig. 6 shows the electroosmotic permeability for three different roughness number density cases. The electroosmotic permeability, κ_e, for the incompressible fluid is defined as:

$$\kappa_e = \frac{\int u_x dA}{E \cdot A}, \tag{33}$$

where u_x is the velocity in x direction (same as the direction of E) and A the area of cross section. Since the generated microstructure of roughness is random, the calculated permeabilities are not exactly the same even though all the parameters are same, but fluctuate around the statistical average. Fig. 6 indicates that the fluctuation decreases as the roughness number density increases for a given total roughness volume fraction. For the current three cases with finite samples, the fluctuation is greater than 6% for n_R =3.6/μm^2 (s_d =0.001), around 3% for n_R=36/μm^2 (s_d=0.01), and less than 1% for n_R=360/μm^2 (s_d=0.1).

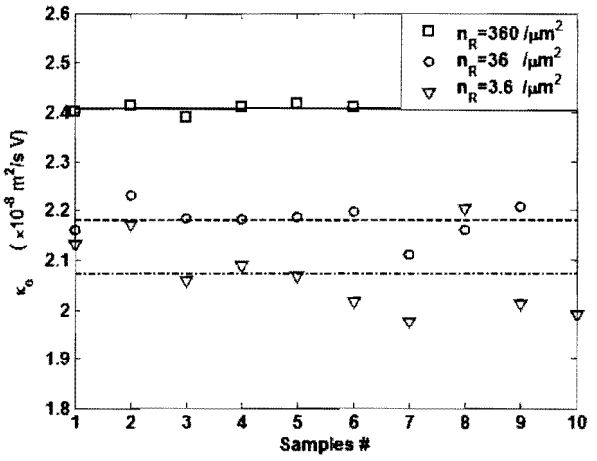

Fig. 6 Electroosmotic permeabilities for three roughness number densities. The symbols are the simulated results for different samples, and the lines represent the statistical average values for each case. The total volume fraction of roughness is 0.05. The bulk ionic concentration n_∞ is 0.3×10^{-5} M.

Fig. 7 shows the calculated electroosmotic permeability when the roughness number densities vary from 3.6 to 1800 /μm^2. The permeability increases with the roughness number density. When a logarithmic scale is used for the x axis, the permeability appears to increase linearly. In other words, the permeability increases with the roughness number density nearly logarithmically.

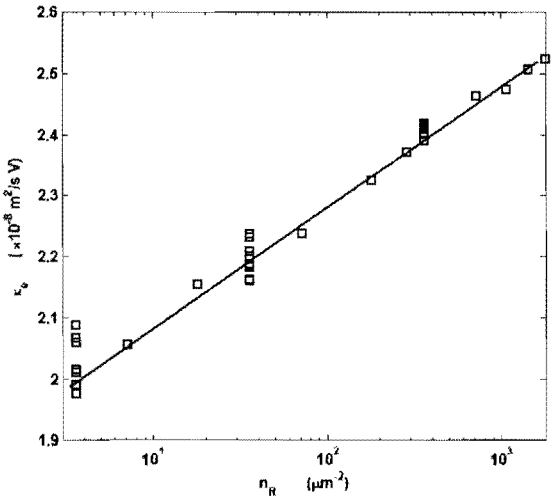

Fig. 7 Electroosmotic permeability versus the roughness number density. The total volume fraction of roughness is 0.05. The bulk ionic concentration n_∞ is 0.3×10^{-5} M. The symbols are the simulated results and the solid line is a linear fit.

B. Roughness volume fraction effect

For the given roughness number density (n_R) and anisotropy parameters, the roughness volume will directly influence the size of roughness elements and therefore the resistance of the channel flow. Fig. 8 shows the electrokinetic permeability when the roughness total volume fraction is changing from 0.01 to 0.09 for two given roughness number densities. There are 1% fluctuation error bars for n_R=360/μm^2 (s_d=0.1) and 3% fluctuations for n_R=36/μm^2 (s_d=0.01). For both cases, the permeability decreases with the roughness total volume fraction. The

permeability difference between the two roughness number densities increases with the roughness volume fraction in the current volume fraction range (0.1~0.9).

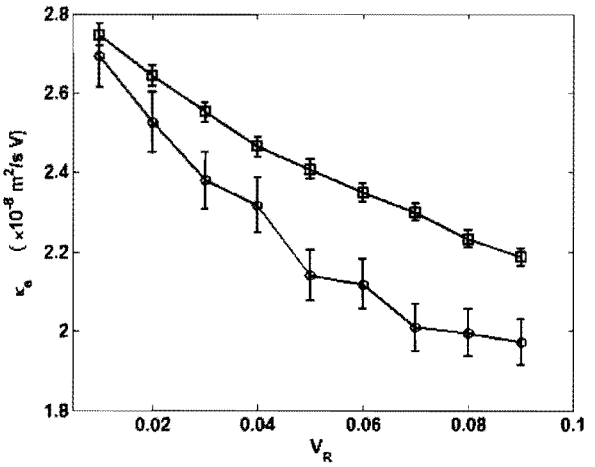

Fig. 8 Electroosmotic permeability in rough microchannels changing with the total roughness volume fraction. The squares are results for n_R=360/μm^2 (s_d=0.1) with 1% fluctuation error bars and the circles are those for n_R=36/μm^2 (s_d=0.01) with 3% fluctuation error bars. The bulk ionic concentration n_∞ is 0.3×10^{-5} M.

C. Anisotropy effect

The anisotropy of the roughness geometry can be controlled by the directional growth probabilities in our generation method. As we mentioned before, the ratio rather than the absolute values of D_j plays the key role in influencing the anisotropy. The directional characteristic length ratio is proportional to the square root of the corresponding directional growth probability. In order to make the anisotropy effects easily understood, we keep the other two directional growth probabilities equal when changing the concerned one. For example, when we consider the y directional anisotropy effect, we keep $D_x : D_y : D_z = 1 : L_y^2 : 1$ and change the

value of L_y^2. For such a case, the L_y will be the value of x axis for y directional characteristic length ratio in Fig. 9.

Fig. 9 shows the electroosmotic permeabilities for different characteristic length ratios in three directions for given roughness number density and roughness volume fraction. First of all, the permeability varies with the directional anisotropy monotonically for all the three directions. The permeability decreases with the z-directional characteristic length (roughness height), yet increases with both x-directional length (roughness length) and y-directional length (roughness width). For the current geometric parameters and electrolyte properties, (1) compared with the isotropic structure case, i.e. the ratio equals unit, the permeability will be lower once the roughness height (z length) is larger; otherwise the permeability will be higher; (2) the larger x-directional length (the fluid direction) will enhance the permeability more than the y-directional length.

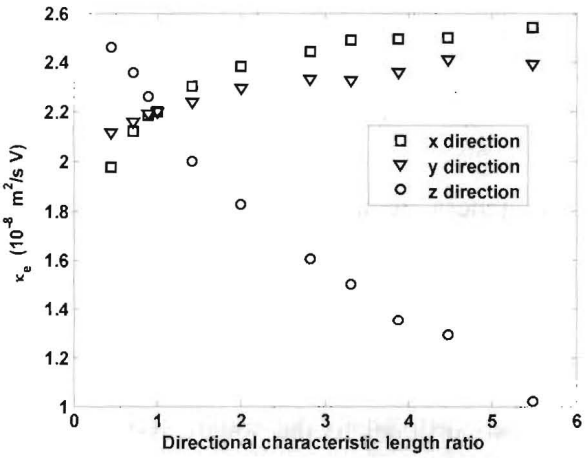

Fig. 9 Anisotropic geometry effects on electroosmotic permeability for different directional characteristic length ratios. The x axis denotes the specified directional characteristic length ratio to the other two ones. The roughness number density n_R=36/μm^2 (s_d=0.01) and the roughness total volume fraction V_R=0.05. The bulk ionic concentration n_∞ is 0.3×10^{-5} M.

D. Debye length effect

Theoretical studies on electroosmotic flows in rough channels have been reported for both thin and thick double layers [28]. However it is a big challenge to do similar analyses when the Debye length is comparable to the characteristic length of roughness because the linear assumptions are not valid any more. Using our numerical framework, we can investigate the Debye length effects on the electroosmotic flows in rough microchannels when the Debye length is close to the roughness size.

We generate the microstructure of a rough microchannel with the parameters: s_d =0.01, $D_x : D_y : D_z$ =1:1:1 and V_R=0.05. The characteristic height of roughness ($L_{roughness}$) can be then calculated from Eq. (13b), i.e. 88.3 nm when the channel width is 1 μm. We change the bulk ionic concentration n_∞ from 3.3 to 0.3 $\times 10^{-5}$ M to vary the dimensionless Debye length ($L_{EDL} / L_{roughness}$) from 0.57 to 1.91.

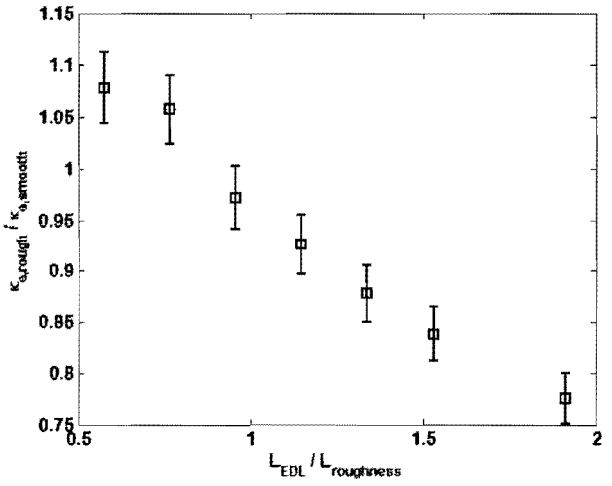

Fig. 10 Dimensionless electroosmotic permeability for different Debye length. The roughness geometry is generated with n_R=36/μm^2 (s_d=0.01) and V_R=0.05, which lead to a fluctuation of

$\kappa_{e,rough}$ at around 3%. The bulk ionic concentration n_∞ varies from 0.3 to 3.3 $\times 10^{-5}$ M to change the Debye length.

The Debye length effect on the electroosmotic permeability in rough microchannels is shown in Fig. 10 when the Debye length is close to the roughness characteristic length. The permeability is also normalized by the corresponding permeability in a smooth channel for the same ionic concentrations. The results indicate: (1) the dimensionless electroosmotic permeability decreases with the dimensionless Debye length monotonically at the current range; (2) the electroosmotic permeability of the rough channel may be greater than that of the smooth channel when the Debye length is smaller than the roughness characteristic length. The reason may lie in the assumption of constant zeta potential for the homogeneously charged surfaces of all roughness elements. In fact the geometric curvature of rough surfaces will lead to an increasing charge density on the surface for a constant zeta potential, which may cause an enhancement of the electroosmotic flow. Therefore the final electroosmotic permeability in a rough channel is influenced by two competing factors from the rough surfaces: enhanced by the increased surface charge density and weakened by the increased geometric resistance. In our case, these two factors obtain a balance when the Debye length is around the roughness characteristic length. Since such a phenomenon has rarely been reported in experimental data, the mechanism will be further investigated in the future work.

V. Conclusions

In this contribution, we developed a numerical framework to model the electrokinetic transport in microchannels with random roughness. The three-dimensional microstructure of the rough channel is generated by a random generation-growth method with three statistical parameters to control the geometric characteristics of the roughness. The governing equations for the

electrokinetic transport are then solved by a high-efficiency lattice Poisson-Boltzmann method in the complex geometries.

The electrokinetic transport in the rough channel is greatly influenced by the geometric characteristics of the roughness. For a given total volume fraction of roughness elements, a higher number density does not only result in a greater electroosmotic permeability through the channel, but also leads to a lower fluctuation due to the random factors. The electroosmotic permeability increases with the roughness number density nearly at a logarithmic law for a given volume fraction of roughness, but decreases with the volume fraction of roughness for a given roughness number density. For both given volume fraction and number density of roughness, the electroosmotic permeability is enhanced by the increases of the characteristic length along the external electric field direction (x) or decreases of the length of the direction across the channel (z). For a given microstructure of rough microchannel, the electroosmotic permeability decreases with the Debye length. Compared with the corresponding flows in a smooth channel, the rough surface may enhance the electrokinetic transport when the Debye length is smaller than the roughness characteristic height under the assumption of constant zeta potential for all surfaces. The present results may improve the understanding of the electrokinetic transport characteristics in microchannels.

Acknowledgement

This work is supported by LANL's LDRD Project 20080727PRD2, through the J. R. Oppenheimer Fellowship awarded to Dr. Wang M. The authors would like to thank Prof. Squires TM, Dr. Wang JK, Prof. Santiago JG and Prof. Li DQ for helpful discussions.

Reference

(1) Squires, T. M.; Quake, S. R. *Reviews of Modern Physics* **2005**, *77*, 977-1026.
(2) Schoch, R. B.; Han, J.; Renaud, P. *Reviews of Modern Physics* **2008**, *80*, 839-883.
(3) Li, D. Q. *Electrokinetics in microfluidics*; Academic: Oxford, 2004.
(4) Stone, H. A.; Stroock, A. D.; Ajdari, A. *Annual Review of Fluid Mechanics* **2004**, *36*, 381-411.
(5) Gui, L.; Ren, C. L. *Langmuir* **2008**, *24*, 2938-2946.
(6) Chrzanowski, W.; Wieckowski, A. *Langmuir* **1998**, *14*, 1967-1970.
(7) Wang, C. Y. *Chemical Reviews* **2004**, *104*, 4727-4765.
(8) Buie, C. R.; Kim, D.; Litster, S.; Santiago, J. G. *Electrochemical and Solid State Letters* **2007**, *10*, B196-B200.
(9) Chen, C. H.; Santiago, J. G. *Journal of Microelectromechanical Systems* **2002**, *11*, 672-683.
(10) Yao, S. H.; Santiago, J. G. *Journal of Colloid and Interface Science* **2003**, *268*, 133-142.
(11) Wang, M.; Wang, J. K.; Chen, S. Y.; Pan, N. *Journal of Colloid and Interface Science* **2006**, *304*, 246-253.
(12) Bazant, M. Z.; Squires, T. M. *Physical Review Letters* **2004**, *92*.
(13) Oddy, M. H.; Santiago, J. G.; Mikkelsen, J. C. *Analytical Chemistry* **2001**, *73*, 5822-5832.
(14) Biddiss, E.; Erickson, D.; Li, D. Q. *Analytical Chemistry* **2004**, *76*, 3208-3213.
(15) Wang, J. K.; Wang, M. R.; Li, Z. X. *Modern Physics Letters B* **2005**, *19*, 1515-1518.
(16) Wong, P. K.; Wang, T. H.; Deval, J. H.; Ho, C. M. *Ieee-Asme Transactions on Mechatronics* **2004**, *9*, 366-376.
(17) Li, D. Q. *Encyclopedia of Microfluidics and Nanofluidics*; Springer Verlag: New York, 2008.
(18) Dutta, P.; Beskok, A. *Analytical Chemistry* **2001**, *73*, 1979-1986.
(19) Li, D. Q. *Colloids and Surfaces a-Physicochemical and Engineering Aspects* **2001**, *195*, 35-57.
(20) Li, B. M.; Kwok, D. Y. *Langmuir* **2003**, *19*, 3041-3048.
(21) Fu, L. M.; Lin, J. Y.; Yang, R. J. *Journal of Colloid and Interface Science* **2003**, *258*, 266-275.
(22) Guo, Z. L.; Zhao, T. S.; Shi, Y. *Journal of Chemical Physics* **2005**, *122*.
(23) Hlushkou, D.; Seidel-Morgenstern, A.; Tallarek, U. *Langmuir* **2005**, *21*, 6097-6112.
(24) Wang, J. K.; Wang, M.; Li, Z. X. *Journal of Colloid and Interface Science* **2006**, *296*, 729-736.
(25) Huang, K. D.; Yang, R. J. *Electrophoresis* **2006**, *27*, 1957-1966.
(26) Butt, H. J.; Graf, K.; Kappl, M. *Physics and chemistry of interfaces*; Wiley-VCH: Weinheim, 2003.
(27) Vourdas, N.; Tserepi, A.; Boudouvis, A. G.; Gogolides, E. *Microelectronic Engineering* **2008**, *85*, 1124-1127.
(28) Dukhin, S. S.; Derjaguin, B. V., Eds. *Electrokinetic phenomena*; Wiley: New York, 1974.
(29) Hu, Y. D.; Werner, C.; Li, D. Q. *Analytical Chemistry* **2003**, *75*, 5747-5758.
(30) Hu, Y. D.; Werner, C.; Li, D. Q. *Journal of Colloid and Interface Science* **2004**, *280*, 527-536.
(31) Hu, Y. D.; Xuan, X. C.; Werner, C.; Li, D. Q. *Microfluidics and Nanofluidics* **2007**, *3*, 151-160.
(32) Das, P. K.; Bhattacharjee, S. *Journal of Colloid and Interface Science* **2004**, *273*, 278-290.
(33) Yang, D. Y.; Liu, Y. *Colloids and Surfaces a-Physicochemical and Engineering Aspects* **2008**, *328*, 28-33.
(34) Wang, M. R.; Wang, J. K.; Chen, S. Y. *Journal of Computational Physics* **2007**, *226*, 836-851.
(35) Lichtner, P. C. *Mat. Res. Soc. Symp. Proc.* **1995**, *353*, 117-130.
(36) Honig, B.; A., N. *Science* **1995**, *268*, 1144-1149.
(37) Wang, M. R.; Wang, J. K.; Pan, N.; Chen, S. Y. *Physical Review E* **2007**, *75*.
(38) Wang, M.; Chen, S. *Journal of Colloid and Interface Science* **2007**, *314*, 264-273.
(39) Chen, S.; Doolen, G. D. *Annual Review of Fluid Mechanics* **1998**, *30*, 329-364.
(40) He, X.; Chen, S.; Doolen, G. D. *Journal of Computational Physics* **1998**, *146*, 282-300.
(41) Wang, J. K.; Wang, M.; Li, Z. X. *Communications in Nonlinear Science and Numerical Simulation* **2008**, *13*, 575-583.
(42) Wang, J. K.; Wang, M.; Li, Z. X. *International Journal of Thermal Sciences* **2007**, *46*, 228-234.

(43) Kang, Q. J.; Zhang, D. X.; Chen, S. Y. *Physical Review E* **2002**, *66*.
(44) Kang, Q. J.; Lichtner, P. C.; Zhang, D. X. *Journal of Geophysical Research-Solid Earth* **2006**, *111*.
(45) Noble, D. R.; Chen, S. Y.; Georgiadis, J. G.; Buckius, R. O. *Physics of Fluids* **1995**, *7*, 203-209.
(46) Inamuro, T.; Yoshino, M.; Ogino, F. *Physics of Fluids* **1995**, *7*, 2928-2930.
(47) Zou, Q. S.; He, X. Y. *Physics of Fluids* **1997**, *9*, 1591-1598.
(48) Rohde, M.; Kandhai, D.; Derksen, J. J.; Van den Akker, H. E. A. *Physical Review E* **2003**, *67*.